2018 25th International Lightning Detection Conference &
7th International Lightning Meteorology Conference
March 12 - 15 | Ft. Lauderdale, Florida, USA

# Characteristics of Lightning Associated with Terrestrial Gamma-ray Flashes in Various Geographical Regions

Bagrat Mailyan[1], Amitabh Nag[1], Ryan K. Said[2], Martin J. Murphy[2], Michael S. Briggs[3], Joseph R. Dwyer[4], Eric Cramer[3], Oliver J. Roberts[5], Matthew Stanbro[3], and Hamid K. Rassoul[1]

[1]Department of Physics and Space Sciences, Florida Institute of Technology, Melbourne, Florida, USA
[2]Vaisala Inc., Louisville, Colorado, USA, [3]The University of Alabama in Huntsville, Huntsville, Alabama,
[4]University of New Hampshire, Durham, New Hampshire, USA, [5]Universities Space Research Association, Huntsville, Alabama, USA

Corresponding author e-mail address: bmailyan@fit.edu; anag@fit.edu

***Abstract*— In this study, we examine the properties of radio frequency (RF) pulses associated with TGFs in various regions of the world. Fermi Gamma-ray Burst Monitor (GBM) provides an unprecedentedly large TGF dataset comprising more than 4000 events allowing for detailed regional studies. We analyze TGFs detected by the Fermi-GBM in conjunction with data from the U.S. National Lightning Detection Network (NLDN) and the Global Lightning Dataset (GLD360). For TGFs occurring within the coverage region of the NLDN, we examine the peak currents reported by the NLDN for 61 pulses that occurred within 5 ms of the start-time of TGFs. Further, using data from the GLD360 we examined the estimated peak currents of RF pulses occurring almost simultaneously with TGFs in Asia, Africa, and the Americas. Peak currents estimated by the NLDN and GLD360 can be viewed as a quantity proportional to the peak magnetic radiation field of RF pulses, rather than their actual peak current. The median absolute peak current in the three regions are 87 kA, 83 kA, and 77 kA, respectively.**

***Keywords—terrestrial gamma rays flashes; lightning; radio frequency pulses; Fermi satellite; lightning locating systems***

## I. INTRODUCTION

Electric and magnetic field waveforms in the radio frequency (RF) range associated with terrestrial gamma-ray flashes (TGFs) have become an important tool for studying this atmospheric phenomenon. The two-dimensional source location of a TGF, observed by the Gamma-ray Burst Monitor (GBM) on-board the low-earth-orbiting Fermi satellite, is obtained by correlating the time-of-occurrence of the TGF with that of the associated RF emission reported by a lightning locating system (LLS) such as the Worldwide Lightning Location Network (WWLLN) [e.g., Connaughton et al., 2010; 2013; Mezentsev et al., 2016]. This narrows down the source location of a TGF from being anywhere within the footprint (a circular region with a radius of 800 km) of the GBM to a specific latitude and longitude. The uncertainty of this location depends upon the location accuracy of the LLS, which can range from a few to greater than 15 km for WWLLN [Mallick et al., 2016], a global long-range LLS operating in the Very Low Frequency (VLF) range.

Connaughton et al. [2013], examined 601 TGF pulses reported by the Fermi-GBM in conjunction with WWLLN-geolocated VLF pulses and found that the rate of association between these two datasets depended strongly upon the duration of the TGF. Short-duration (less than 200 μs) TGFs were more likely to be associated with WWLLN RF pulses than longer duration TGFs. These short-duration TGFs had an average WWLLN-estimated far-field energy that was significantly higher than that for longer-duration TGFs. Connaughton et al. [2013] interpreted WWLLN-reported RF pulses occurring almost simultaneously (within 200 μs) with GBM-reported TGF photon-count peak-times to be the VLF signature of relativistic electrons and their resulting ionization. On the other hand, RF pulses occurring within a longer time-window of 20 ms of the TGF peak-times were thought to be produced by lightning occurring in the same thunderstorm system as the TGF. According to the model developed by Dwyer and Cummer [2013], shorter duration TGFs will produce VLF signatures with higher radiation field peaks which are proportional to the time derivative of the current moment produced by the electron avalanche.

Splitt et al. [2010] qualitatively showed that TGFs occur preferentially over coastal regions, large islands, peninsulas

and isthmuses in tropical regions where lightning occurrence rates are high. Regional variations in TGF occurrence rates have also been examined by Smith et al. [2010], Fuschino et al. [2011] and Briggs et al. [2013]. In this study, we examine the peak currents of RF pulses geolocated by the NLDN associated with 44 TGFs reported by the Fermi-GBM between January, 2014 and July, 2016. Additionally, we examine the GLD360-estimated peak currents of TGF-associated RF pulses for TGFs reported by the Fermi-GBM during 2013-2017 in different parts of the world. Note that the NLDN- and GLD360-estimated peak current of an RF pulse is simply an indication of its magnetic field peak amplitude.

## II. Instrumentation and Data

The GBM is an auxiliary instrument onboard the Fermi Gamma-ray Space Telescope comprising of two bismuth germanate (BGO) and 12 sodium iodide (NaI) detectors [Meegan et al., 2009]. Particles with effective energy ranges of 10-1000 keV and 0.2-40 MeV are measured by the sodium iodide (NaI) and BGO detectors, respectively. The timing precision of the measurements is 2 μs, while absolute accuracy is several microseconds. The broad energy range of the BGO detectors along with a low dead time of 2.6 μs make them well-suited for studying sub-millisecond TGFs with energies of up to tens of MeV. The Fermi-GBM is capable of measuring TGFs within a horizontal distance of up to about 800 km from the spacecraft's footprint [Roberts et al., 2018]. After implementation of new ground-search algorithms in 2012, the TGF detection rate improved to about 800 events per year, making the GBM the most efficient current-generation TGF observatory [Briggs et al., 2013]. The Fermi-GBM TGF catalog provides the photon counts per 2 μs for each of the two BGO detectors, cumulative photon counts for the 12 NaI detectors per 2 μs (10 μs if NaI detectors are saturated), spacecraft position, TGF start-time measured at the spacecraft altitude, and the duration of the discovery-bin. The discovery-bin is the time-window in the ground-search algorithm corresponding to the most significant joint Poisson probability of occurrence of the identified TGF [Briggs et al., 2013; Roberts et al., 2018]. The TGF start-time in the catalog is defined as the start-time of this discovery-bin. The discovery-bin start-time is a reasonable approximation for the TGF photon flux start-time.

The U.S. NLDN uses ground-based electric and magnetic field sensors operating in the predominantly-low-frequency (LF) range (400 Hz to 400 kHz) to measure electromagnetic field changes produced by lightning discharges and geolocates these discharges using time-of-arrival and magnetic direction finding techniques [Cummins and Murphy, 2009; Nag et al., 2015]. In some cases, other types of atmospheric electrical discharges such as TGFs that may produce relatively high-amplitude LF signatures are detected and geolocated by the NLDN. In addition to the time (the start-time of the LF pulse) and two-dimensional location (along with an estimated location error) of the sources of these pulses, the NLDN also provides information on their polarity and peak current. Magnetic field LF waveform characteristics such as rise time and peak-to-zero time of pulses are reported by individual sensors and geolocated events are classified by the network as IC pulses or CG return strokes based on their waveform characteristics. After a network-wide upgrade in 2013, the NLDN IC flash detection efficiency is about 50% [Murphy and Nag, 2015]. The detection efficiency for negative first strokes in Gainesville, Florida region was reported to be about 98%, the IC flash and return-stroke classification accuracy was reported to be 95% and 92% respectively [Zhu et al., 2016a; 2016b]. The location accuracy for CG strokes is expected to be about a few hundred meters [Nag et al., 2015]. The polarity estimation accuracy of the NLDN is close to 100% [Nag et al., 2015].

In the south, the coverage region of the NLDN extends to (going from east to west) the Bahamas, northern Mexico, and northern Baja California, beyond which the detection efficiency of the network decreases. The Fermi spacecraft has a low-Earth circular orbit. Its orbital inclination, which is the northern-most and southern-most latitude over which Fermi's footprint passes, is 25.6 degrees. The 25.6° N latitude is indicated with a red line in Figure 1. TGFs that occur as far as a few hundred kilometers north of this latitude may be detected by the Fermi-GBM. For our analysis, we used a region (shown in Figure 1) over which we expect the coverage of the NLDN and the Fermi-GBM to overlap. In this region, we identified 44 GBM-reported TGFs occurring between January, 2014 and July, 2016 for which the NLDN geolocated one or more "lightning events" (RF pulses) occurring within 5 ms of the start-time of the TGF discovery-bin (or TGF start-time). There were 61 such NLDN-reported RF pulses of which 22 pulses occurred almost simultaneously (within 200 μs) with 21 TGFs. Note that two NLDN-reported pulses occurred 5 μs before and 22 μs after the start-time of one of the TGFs respectively. In Figure 1, we show the NLDN-locations of the 61 RF pulses occurring within 5 ms of the TGF start-time. In order to account for the propagation delay between the locations of the TGF source and the spacecraft, a "light travel time correction" is applied to the spacecraft-reported times. To calculate this correction, we assume that the locations of these NLDN RF pulses are the two-dimensional locations of the TGF sources. This assumption is more robust if the RF pulses are signatures of the TGFs themselves rather than of lightning occurring in spatial and temporal proximity of these TGFs. The altitude of the TGF sources is assumed to be 12 km. Then the distance between the TGF source locations and the spacecraft location is determined, from which the propagation delay is calculated (e.g., Briggs et al, 2010). Note that, if this light travel time correction is not applied timing errors of the order of a few milliseconds can occur.

The Global Lightning Dataset (GLD360) is a global lightning detection network, which has been in operation since September 2009, with data being made available to users since May 2011. The GLD360 employs VLF sensors placed at locations around the world. The stroke locations are obtained using both time-of-arrival and magnetic-direction-finding methods in conjunction with a lightning waveform recognition algorithm [Said et al., 2010]. The GLD360 also reports the

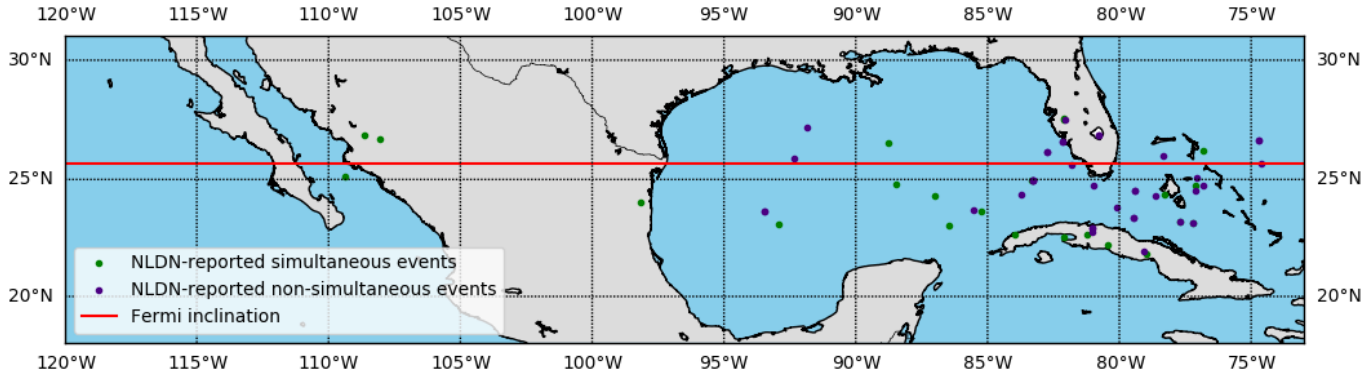


Fig. 1. Map showing locations of 61 NLDN-reported events (RF pulses) that occurred within 5 ms of 44 TGFs reported by the Fermi-GBM. Green dots (NLDN-reported simultaneous events) indicate the locations of 22 pulses occurring within 200 μs of 21 TGFs. Purple dots (NLDN-reported non-simultaneous events) indicate the locations of 39 pulses occurring in the 200 μs – 5 ms time window before or after the other 23 TGFs. The red line indicates the 25.6° N orbital inclination of Fermi. Note that some dots overlap with each other due to the spatial proximity of their locations.

peak current (inferred from the measured magnetic field peak) and polarity. The latter is influenced by ionospheric reflections and determined via the cross correlation with the bank of "canonical" waveforms. In this study, we use five years (2013-2017) of GLD360 data to examine TGF-associated pulses in the different regions across the world. GLD360 reported RF pulses whose start times were within 3.5 ms of the GBM-reported TGFs start time were included in our analysis.

## III. TGF-Associated Radio Frequency Pulses Observed by the NLDN

We examined the time intervals between the NLDN-reported pulse start-times and the GBM-reported TGF start-times for 61 RF pulses associated with 44 TGFs. For 21 out of the 61 (about 34%) RF pulses, the NLDN-reported start-times preceded the respective TGF's start-times reported by the GBM. The time-intervals for those 21 pulses ranged from 5 μs to about 2.9 ms, with the median being 1.1 ms. For 40 RF pulses (about 66%) whose start-times were after the respective TGF's start-time, the time-intervals ranged from 3.4 μs to 4.5 ms with the median being 401 μs. Twenty six (43%) of the 61 RF pulses were classified by the NLDN as CG strokes. Eight (13%) pulses had negative initial polarity. For 21 out of 44 (48%) TGFs, the start-times of one or two (for TGF09 only as mentioned in section 2) RF pulses occurred nearly simultaneously (within 200 μs) with the respective TGF's start-time. For these TGFs, the median absolute time interval between the NLDN-reported pulse start-time and the respective TGF's start-time is 50 μs. 16 out of 22 (73%) RF pulses started after the TGF start-time. Eighteen out of these 22 (about 82%) pulses were classified by the NLDN as CG strokes. Six out of 22 (27%) of these pulses had negative initial polarity.

Figure 2 shows the scatter plot of the NLDN-estimated peak currents for the 61 RF pulses versus the NLDN-TGF time-intervals. Pulses that were classified by the NLDN as CG strokes are shown using squares and those classified as IC pulses are shown using circles. The NLDN-estimated peak currents can be viewed as a quantity proportional to the peak magnetic radiation field of these pulses, rather than their actual peak current. The NLDN classified 26 of the 61 (43%) pulses as CG, with absolute value of peak currents ranging from 13 kA to 166 kA and the median being 24 kA. Thirty five (57%) pulses were classified as IC, with their absolute peak currents ranging from 4 kA to 205 kA and the median being 11 kA. For the 22 RF pulses that occurred nearly simultaneously with TGFs (200-μs time-window between the two vertical dashed lines in Figure 2), the absolute value of the peak current ranged from 13 to 205 kA, with the median being 26 kA. Seventeen (about 77%) of these pulses had peak currents less than 50 kA. The absolute value of the peak currents for pulses that were not simultaneous with TGFs, but within 5 ms of one, ranged from 4 to 87 kA with the median being 11 kA. This median peak current is two-and-half times smaller than the median peak current of the simultaneous RF pulses. 8 out of 39 (21%) of these non-simultaneous pulses were classified by the NLDN as CG. Two pulses out of 39 (5.1%) had negative initial polarity.

## IV. TGF-Associated Radio Frequency Pulses Observed by the GLD360

We examined the time intervals between the GLD360-reported pulse start-times and the GBM-reported TGF start-times for 2273 RF pulses associated with 2198 TGFs. Figure 3 shows the scatter plot of the GLD360-estimated peak currents for the 2273 RF pulses versus the GLD360-TGF time-intervals. For 442 out of the 2273 (about 20%) RF pulses, the GLD360-reported start-times preceded the respective TGF's start-times reported by the GBM. The time-intervals for those 448 pulses ranged from 1 μs to about 3.4 ms, with the median being 65 μs. For 1825 RF pulses (about 80%) whose start-times were after the respective TGF's start-time, the time-intervals ranged from 1 μs to 3.5 ms with the median being 91

μs. 922 (41%) pulses had negative initial polarity. For 1505 out of 2198 (68%) TGFs, the start-times of RF pulses occurred nearly simultaneously (200-μs time-window between the two vertical dashed lines in Figure 3) with the respective TGF's start-time. For these TGFs, the median absolute time interval between the GLD360-reported pulse start-time and the respective TGF's start-time is 55 μs. This is similar to the 50 μs RF pulse-TGF time interval for simultaneous pulses reported by the NLDN. 1246 out of 1547 (81%) RF pulses started after the TGF start-time. 654 out of 1547 (42%) of these pulses had negative initial polarity.

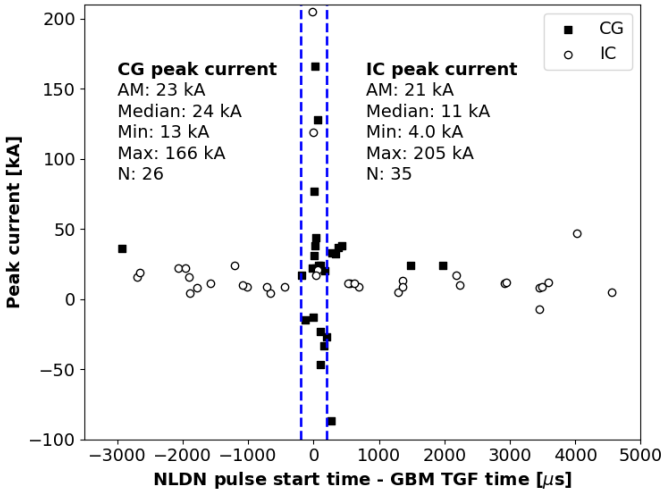


Fig. 2. Scatter plot showing the NLDN-estimated peak currents for 61 RF pulses versus the NLDN-TGF time-intervals. Pulses that were classified by the NLDN as CG strokes are shown using black squares and those classified as IC pulses are shown using white circles. Vertical dashed lines indicate the 200-μs time window within which RF pulses were essentially simultaneous with TGFs. The arithmetic mean (AM), median, minimum, and maximum are shown for the absolute values of the peak currents.

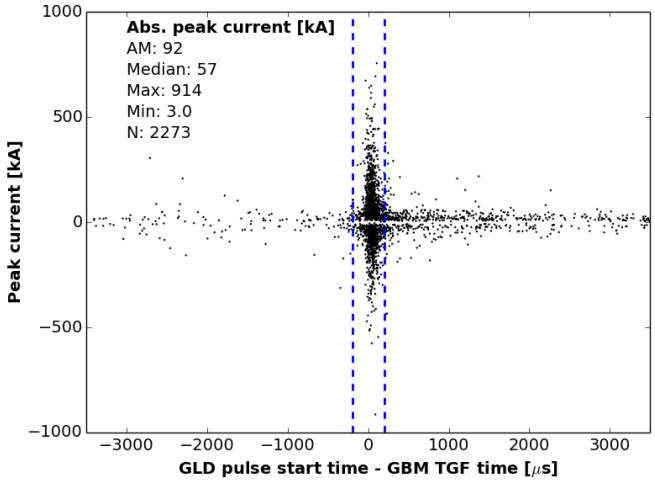


Fig. 3. Scatter plot showing the GLD360-estimated peak currents for RF pulses versus the pulse-start-to-TGF-start time-intervals. Vertical dashed lines indicate the 200-μs time window within which RF pulses were essentially simultaneous with TGFs. The arithmetic mean (AM), median, minimum, and maximum are shown for the absolute values of the peak currents.

Figures 4 and 5 show the histogram of the GLD360-estimated peak currents for RF pulses that were simultaneous and non-simultaneous (occurring in the 200 μs to 3.5 ms time-window before or after TGFs) with TGFs, respectively. The GLD360-estimated peak currents can be viewed as a quantity proportional to the peak magnetic radiation field of these pulses, rather than their actual peak current. For the positive polarity pulses, GLD360-estimated peak currents ranged from 3 kA to 756 kA with the median being 55 kA. The peak currents for negative polarity pulses ranged from 4 kA to 914 kA with the median being 59 kA. For the 1547 RF pulses that occurred nearly simultaneously with TGFs, the absolute value of the peak currents ranged from 3 to 914 kA, with the median being 82 kA. 438 (28%) of these pulses had peak currents less than 50 kA. 1160 out of 1547 (75%) RF pulses had peak currents with absolute values less than 150 kA. The absolute value of the peak currents for 726 pulses that were not simultaneous with TGFs, but within 3.5 ms of one, ranged from 4 to 435 kA with the median being 26 kA. This median peak current is roughly three times smaller than the median peak current of the simultaneous RF pulses. 268 out of 726 (37%) of these non-simultaneous pulses had negative initial polarity.

Figures 6, 7, and 8 show the histograms of peak currents of RF pulses that occurred simultaneously with TGFs in three different regions: Asia (60° E to 180° E), Africa (30° W to 60° E), and the Americas (180° W to 30° W), respectively. The latitudinal limits for each of our regions was 30° N to 30° S. The median absolute peak current in the three regions are 87 kA, 83 kA, and 77 kA, respectively. It appears that there is not much difference in the peak currents of TGF-associated RF pulses between the different regions.

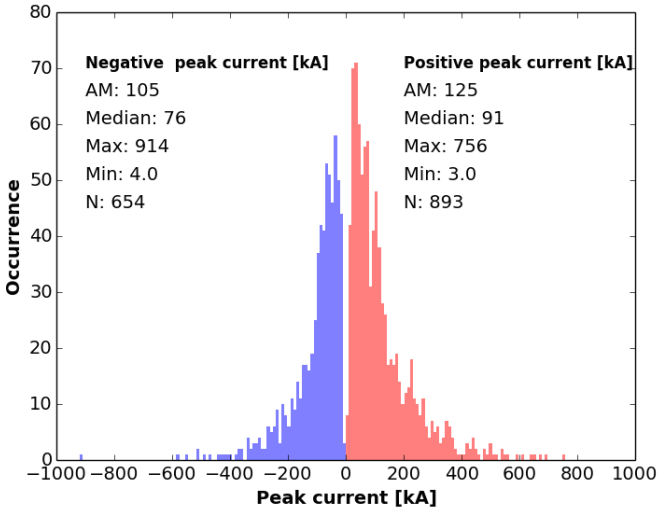


Fig. 4. Histogram of GLD360-estimated peak currents of RF pulses occurring simultaneously with TGFs during 2013-2017.

## V. Disscussion and Summary

We examined the peak current and polarity of RF pulses geolocated by the NLDN associated with 44 TGFs reported by the Fermi-GBM between January, 2014 and July, 2016. There were 61 such NLDN-reported RF pulses of which 22 pulses

occurred almost simultaneously (within 200 μs) with 21 TGFs. The median peak currents for pulses that were simultaneous with TGFs was 26 kA versus 11 kA for pulses that were not simultaneous with TGFs (but occurred within 5 ms of one. While the majority of the simultaneous RF pulses had positive initial polarity, 27% had negative initial polarity. To the best of our knowledge, all previous studies have reported the polarity of TGF-associated IC or CG lightning to be positive. This indicates that negative charge can move in either upward or downward directions during TGFs. We speculate that these RF pulses are signatures of either the relativistic electron avalanches associated with TGFs or currents traveling in conductive paths "pre-conditioned" by TGF-associated relativistic electron beams between cloud charge regions of opposite polarity.

We examined the GLD360-estimated peak currents of TGF-associated RF pulses for TGFs reported by the Fermi-GBM during 2013-2017 in different parts of the world. For the 1547 RF pulses that occurred nearly simultaneously with TGFs, the absolute value of the peak currents ranged from 3 to 914 kA, with the median being 82 kA. 42% of these pulses had negative initial polarity. It appears that there is not much difference in the peak currents of TGF-associated RF pulses between the Asian, African, and American regions examined in this study.

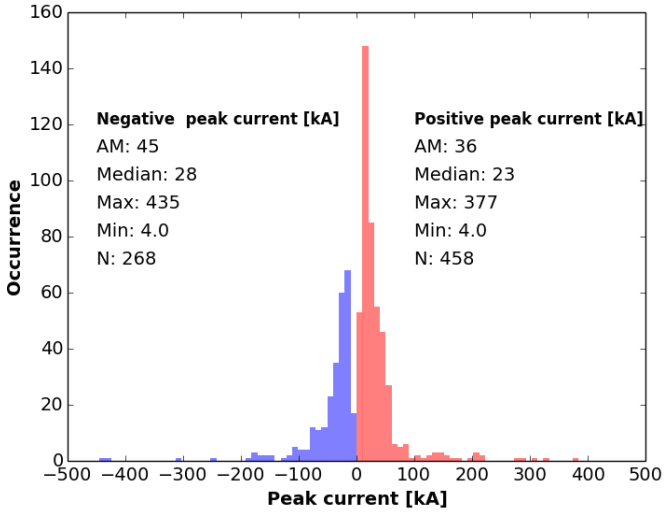


Fig. 5. Histogram of GLD360-estimated peak currents of RF pulses occurring non-simultaneously with TGFs during 2013-2017.

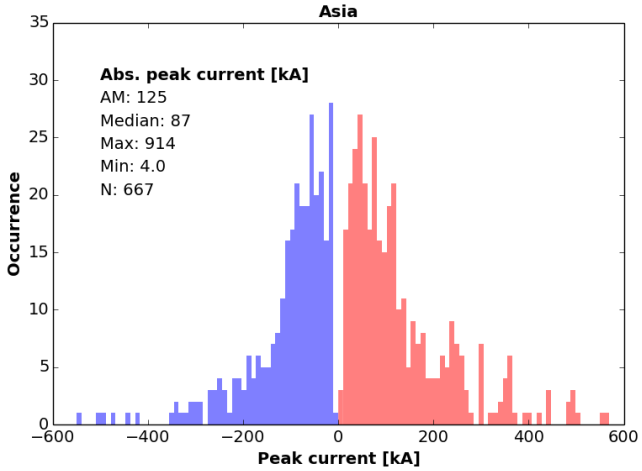


Fig. 6. Histogram of GLD360-estimated peak currents of RF pulses occurring simultaneously with TGFs in the Asian region during 2013-2017. Note that the horizontal axis is truncated at 600 kA because only six pulses has peak current above that limit.

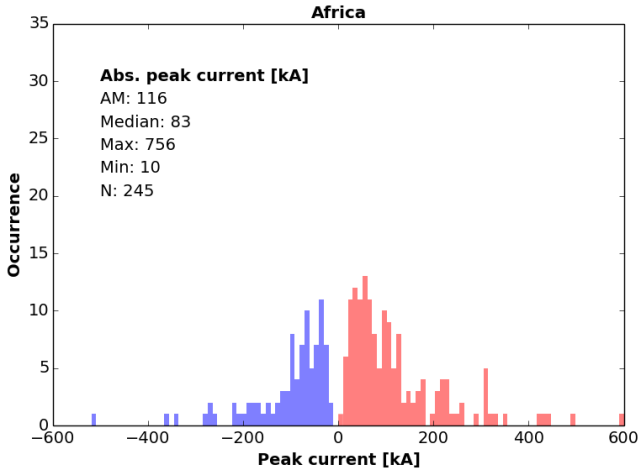


Fig. 7. Histogram of GLD360-estimated peak currents of RF pulses occurring simultaneously with TGFs in the African region during 2013-2017. Note that the horizontal axis is truncated at 600 kA because only one pulse has peak current above that limit.

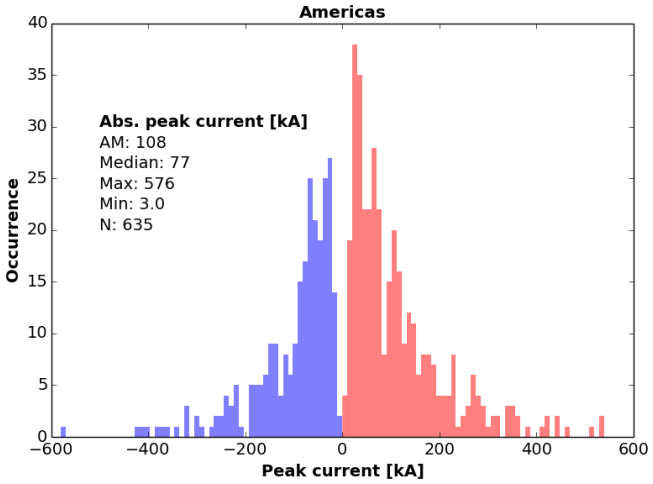


Fig. 8. Histogram of GLD360-estimated peak currents of RF pulses occurring simultaneously with TGFs in the Americas region during 2013-2017.

## ACKNOWLEDGMENT

The authors would like to thank Vaisala Inc. for the NLDN and GLD360 data. The Fermi-GBM TGF data is available at (http://fermi.gsfc.nasa.gov/ssc/data/access/gbm/tgf/). This work was supported in part by AFOSR grant FA9550-16-1-0396.

## REFERENCES

Brophy, J. G., E. M. Klein, and M. A. Stewart (1999), Textural (Nomarski interferometry) studies of plagioclase phenocryst zonation styles in MORB dikes and lavas from the north wall of the Hess Deep Rift, Eos Trans. AGU, 80(46), Fall Meet. Suppl., F985.

Briggs, M., G. Fishman, V. Connaughton, P. N. Bhat, W. Paciesas, R. Preece, C. Wilson-Hodge, V. Chaplin, R. Kippen, A. von Kienlin, et al. (2010), First results on terrestrial gamma ray flashes from the Fermi Gamma-ray Burst Monitor, Journal of Geophysical Research: Space Physics (1978–2012), 115 (A7).

Briggs, M. S., S. Xiong, V. Connaughton, D. Tierney, G. Fitzpatrick, S. Foley, J. E. Grove, A. Chekhtman, M. Gibby, G. J. Fishman, et al. (2013), Terrestrial gamma-ray flashes in the Fermi era: Improved observations and analysis methods, Journal of Geophysical Research: Space Physics, 118 (6), 3805–3830.

Connaughton, V., M. Briggs, R. Holzworth, M. Hutchins, G. Fishman, C. Wilson-Hodge, V. Chaplin, P. N. Bhat, J. Greiner, A. von Kienlin, et al. (2010), Associations between Fermi Gamma-ray Burst Monitor terrestrial gamma ray flashes and sferics from the World Wide Lightning Location Network, Journal of Geophysical Research: Space Physics (1978– 2012), 115 (A12).

Connaughton, V., M. S. Briggs, S. Xiong, J. R. Dwyer, M. L. Hutchins, J. E. Grove, A. Chekhtman, D. Tierney, G. Fitzpatrick, S. Foley, S. McBreen, P. N. Bhat, V. L. Chaplin, E. Cramer, G. J. Fishman, R. H. Holzworth, M. Gibby, A. von Kienlin, C. A. Meegan, W. S. Paciesas, R. D. Preece, and C. Wilson-Hodge (2013), Radio signals from electron beams in terrestrial gamma-ray flashes, J. Geophys. Res. Space Physics, 118, 2313–2320, doi:10.1029/2012JA018288.

Cummins, K., and M. Murphy (2009), An overview of lightning locating systems: History, techniques, and data uses, with an in-depth look at the US NLDN, IEEE Trans. Electromag. Compat., 51(3), 499–518, doi:10.1109/TEMC.2009.2023450.

Dwyer, J. R., and S. A. Cummer (2013), Radio emissions from terrestrial gamma-ray flashes, Journal of Geophysical Research: Space Physics, 118 (6), 3769–3790.

Fuschino, F., et al. (2011), High spatial resolution correlation of AGILE TGFs and global lightning activity above the equatorial belt, Geophys. Res. Lett., 38, L14806, doi:10.1029/2011GL047817.

Mallick, S., V. Rakov, T. Ngin, W. Gamerota, J. Pilkey, J. Hill, M. Uman, D. Hordan, M. Hutchins, and R. Holzworth (2014a), Evaluation of the WWLLN performance characteristics using rocket-triggered lightning data, in Intl. Conf. on Grounding and Earthing/6th Intl. Conf. on Lightning Physics and Effects.

Meegan, C., G. Lichti, P. N. Bhat, E. Bissaldi, M. S. Briggs, V. Connaughton, R. Diehl, G. Fishman, J. Greiner, A. S. Hoover, et al. (2009), The Fermi Gamma-ray Burst Monitor, The Astrophysical Journal, 702 (1), 791.

Mezentsev, A., N. Østgaard, T. Gjesteland, K. Albrechtsen, N. Lehtinen, M. Marisaldi, D. Smith, and S. Cummer (2016), Radio emissions from double RHESSI TGFs, Journal of Geophysical Research: Atmospheres, 121 (13), 8006–8022.

Nag, A., M. J. Murphy, W. Schulz, and K. L. Cummins (2015) Lightning locating systems: Insights on characteristics and validation techniques, Earth and Space Science, 2, doi:10.1002/2014EA000051.

Roberts, O. J., G. Fitzpatrick, M. Stanbro, M. Briggs, S. McBreen, J. E. Grove, R. Holzworth, A. Chekhtman, E. Cramer, and B. Mailyan (2018), The First Fermi-GBM Terrestrial Gamma-ray Flash Catalog, submitted to JGR space physics.

Said, R. K., M. J. Murphy, N. Demetriades, U. S. Inan, and K. L. Cummins (2010), Initial performance estimates of the GLD360 lightning detection network, Abstract #AE33A-0255 presented at 2010 Fall Meeting, AGU, San Francisco, Calif.

Smith, D. M., B. J. Hazelton, B. W. Grefenstette, J. R. Dwyer, R. H. Holzworth, and E. H. Lay (2010), Terrestrial gamma ray flashes correlated to storm phase and tropopause height, J. Geophys. Res., 115, A00E49, doi:10.1029/2009JA014853.

Splitt, M. E., S. M. Lazarus, D. Barnes, J. R. Dwyer, H. K. Rassoul, D. M. Smith, B. Hazelton, and B. Grefenstette(2010), Thunderstorm characteristics associated with RHESSI identified terrestrial gamma ray flashes, J. Geophys. Res., 115, A00E38, doi:10.1029/2009JA014622.